2007 Mediterranean Conference on Control and
Automation, July 27 - 29, 2007, Athens - Greece

Active Suspensions: A Reduced-Order $\mathscr{H}_\infty$ Control Design Study

J. Wang*, A. C. Zolotas†, D. A. Wilson‡

*Department of Automation
Tsinghua University, Beijing 100084, P. R. China
junwang@tsinghua.edu.cn
†Department of Electronic and Electrical Engineering
Loughborough University, Loughborough, Leicestershire LE11 3TU, UK
a.c.zolotas@lboro.ac.uk
‡School of Electronic & Electrical Engineering
The University of Leeds, Leeds LS2 9JT, UK
D.A.Wilson@leeds.ac.uk

***Abstract*— This paper studies order reduction issues for a vehicle active suspension system throughout its modelling, H-infinity controller design and controller refinement. Computer simulations demonstrate that an H-infinity controller for a full active suspension can be significantly reduced to nearly one third of its full order, while the active suspension performance is only slightly degraded. As a by-product, this paper also provides an explicit algorithm for reduced H-infinity control for singular and non-singular continuous-time systems.**

I. Introduction

The majority of strategies for active suspensions involve observer-based, optimal and robust control, but their application in engineering practice is hindered by the resulting high order controllers. Among the over two thousand publications on active suspension control, only a few address the order reduction issue. In [1], Hankel norm reduction method was applied to a half vehicle together with a comparison with other model reduction methods. In [2] the order of a quarter-vehicle suspension model was reduced by analysing the dominant states of the nonlinear model. In [3] the singular perturbation method was applied to a full-vehicle suspension model. In [4] an empirical Gramian balanced model-reduction strategy was utilised to reduce a nonlinear quarter-vehicle suspension model. In [5], [6], [7], a full suspension model was decoupled into two half models or four quarter models, which reduced model orders but increased the number of controllers.

Reduced $\mathscr{H}_\infty$ control has been studied for over a decade, and majority of the research has been on singular systems [8], [9]. With the application of linear matrix inequality (LMI) techniques to $\mathscr{H}_\infty$ control, research has moved increasingly to LMI-based $\mathscr{H}_\infty$ reduced control problems [10], [11], [12]. More recently, [13] presented a unified method for reduced $\mathscr{H}_\infty$ control for both continuous- and discrete-time *general* systems. In [13], only a very simple numerical example was demonstrated. It is therefore of interest to investigate the applicability of this theory to a practical engineering problem, such as an active suspension system, and this is one of motivations for carrying out the research presented in this paper.

Compared to reduced $\mathscr{H}_\infty$ control, general model reduction problems have been studied since the emergence of the modern control theory. Reduction techniques can be generally classified into two categories: (i) direct methods, i.e. direct reduced controller design, and (ii) non-direct methods, i.e. model reduction before a design or a controller reduction after. It is of interest to see how these methods can work together throughout the whole process of active suspension system design, and this also motivated the research.

The paper is organised as follows: Section II presents the full suspension system model and its approximation via model reduction. Section III presents an explicit algorithm for reduced $\mathscr{H}_\infty$ control and applies it to the reduced-order suspension system model to obtain a reduced $\mathscr{H}_\infty$ controller (with further controller reduction using the balanced truncation method). The controller is assessed by computer simulations in Section IV. Finally, concluding remarks are made and future research directions are mapped out in Section V.

The following notation is used in this paper, $\mathbf{I}$ and $\mathbf{0}$ denote a unit and a zero matrix respectively. The dimension subscript of the matrices will be added if necessary. For a matrix A, $\mathrm{rank}(A)$ is its rank, $\sigma_i(A)$ is its i^{th} Hankel singular value, A^T is its transpose, $A^\perp$ is its orthogonal complement and A^+ is its pseudo inverse. $\mathbf{Sym}(A,X,B)$ is defined as $AXB+(AXB)^T$. For a system, $\|\cdot\|_\infty$ stands for its $\mathscr{H}_\infty$ norm, and $\|\cdot\|_H$ for Hankel norm. The lower linear fractional transformation between two systems G and K is denoted by $\mathscr{F}_l(G,K)$.

II. Suspension System Modelling

A. Modelling of Full Vehicle Active Suspensions

A schematic diagram of a full-vehicle model with an active suspension system [14] is shown in Fig. 1.

Each quarter of the active suspension consists of a spring, a damping valve and a force generator connected in parallel. The force generator is regulated by a controller

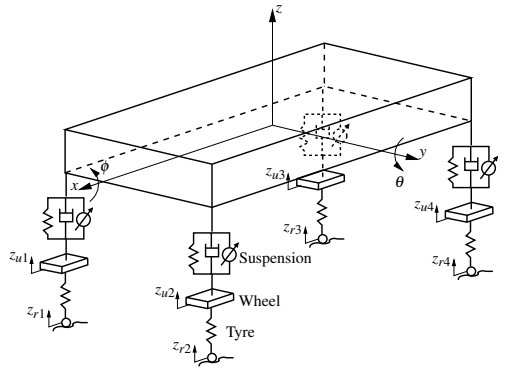

Fig. 1. Schematic diagram of a full-vehicle model

to improve vehicle ride and handling, while the spring and damper are employed to suppress high frequency vibration above the bandwidth of the force generator.

TABLE I

VEHICLE MODEL SYMBOLS AND VALUES

Symbols	Physical meanings	Value	Unit
m_s	sprung mass	1500	kg
I_x	roll moment of inertial	460	kg m^2
I_y	pitch moment of inertial	2160	kg m^2
$m_{u1\sim4}$	unsprung mass	59	kg
$c_{s1\sim2}$	suspension damping ratio	1000	Ns/m
$c_{s3\sim4}$	suspension damping ratio	1100	Ns/m
$k_{s1\sim2}$	suspension stiffness	35000	N/m
$k_{s3\sim4}$	suspension stiffness	38000	N/m
k_u	tyre stiffness	190000	N/m
$z_{us1\sim4}$	suspension deflection		
$z_{u1\sim4}$	wheel vertical displacement		
$z_{r1\sim4}$	vertical road displacement		
$z_{ru1\sim4}$	tyre deflection		
$F_{1\sim4}$	actuator force		

The symbols and parameters of the vehicle model are listed in Table I and the differential equations can be derived straightforwardly as given in [1], [14].

By choosing the following vectors of state, disturbance and control signals

$$\mathbf{x} = \begin{bmatrix} z & \dot{z} & \theta & \dot{\theta} & \phi & \dot{\phi} & z_{u1} & \dot{z}_{u1} & z_{u2} & \dot{z}_{u2} & z_{u3} & \dot{z}_{u3} & z_{u4} & \dot{z}_{u4} \end{bmatrix}^T$$
$$\mathbf{w} = \begin{bmatrix} z_{r1} & z_{r2} & z_{r3} & z_{r4} & M_r \end{bmatrix}^T$$
$$\mathbf{u} = \begin{bmatrix} F_1 & F_2 & F_3 & F_4 \end{bmatrix}^T$$

we obtain the state equation for the active suspension system

$$\dot{\mathbf{x}} = \mathbf{A}\mathbf{x} + \mathbf{B_w}\mathbf{w} + \mathbf{B_u}\mathbf{u} \tag{1}$$

The ride comfort is quantified by the power of weighted vehicle body acceleration $\ddot{z}$, $\ddot{\theta}$ and $\ddot{\phi}$. In addition, we need to constrain force generated by actuators. Hence we choose the vector of regulated output variables as

$$\mathbf{z} = \begin{bmatrix} \ddot{z} & \ddot{\theta} & \ddot{\phi} & F_1 & F_2 & F_3 & F_4 \end{bmatrix}^T$$

The most common sensors for active suspension control are accelerometers and gyrometers [15]. In this paper, we choose the vector of measuring signals as

$$\mathbf{y} = \begin{bmatrix} \ddot{z} & \dot{\theta} & \dot{\phi} \end{bmatrix}^T$$

Combined with the state equation given in (1), a state-space model $\mathbf{G_{gel}}$ for the integrated active suspension control is formulated as follows:

$$\begin{cases} \dot{\mathbf{x}} &= \mathbf{A}\mathbf{x} + \mathbf{B_w}\mathbf{w} + \mathbf{B_u}\mathbf{u} \\ \mathbf{z} &= \mathbf{C_z}\mathbf{x} + \mathbf{D_{zw}}\mathbf{w} + \mathbf{D_{zu}}\mathbf{u} \\ \mathbf{y} &= \mathbf{C_y}\mathbf{x} + \mathbf{D_{yw}}\mathbf{w} + \mathbf{D_{yu}}\mathbf{u} \end{cases} \tag{2}$$

where the matrices $\mathbf{C_z}$, $\mathbf{C_y}$, $\mathbf{D_{zw}}$, $\mathbf{D_{zu}}$, $\mathbf{D_{yw}}$ and $\mathbf{D_{yu}}$ are obtained in a straightforward manner. Then the passive suspension system model $\mathbf{G_{pss}}$ is

$$\begin{cases} \dot{\mathbf{x}} &= \mathbf{A}\mathbf{x} + \mathbf{B_w}\mathbf{w} \\ \mathbf{z} &= \mathbf{C_z}\mathbf{x} + \mathbf{D_{zw}}\mathbf{w} \end{cases} \tag{3}$$

In this paper, we choose the following scaling matrices for $\mathbf{w}$ and $\mathbf{z}$ to get a normalised system:

$$\mathbf{S_w} = \mathrm{diag}(0.0014, 0.0014, 0.0014, 0.0014, 500)$$
$$\mathbf{S_z} = 10^{-3} \cdot \mathrm{diag}(280.0, 840.0, 280.0, 0.3, 0.3, 0.3, 0.3)$$

As human sensitivity to vibration depends on frequency [16], we follow [17] and choose the following weighting functions for $\ddot{z}$, $\ddot{\theta}$ and $\ddot{\phi}$:

$$W_{\ddot{z}} = \frac{s^2 + 314.2s + 987}{s^2 + 43.98s + 987},\ W_{\ddot{\theta}} = W_{\ddot{\phi}} = \frac{s^2 + 50.27s + 25.27}{s^2 + 7.037s + 25.27}$$

Since we do not have any particular frequency requirements on actuator force, we simply choose $W_u = 1$ as its weighting function. In summary, the weighting function matrix for the regulated output $\mathbf{z}$ is

$$\mathbf{W_z} = \mathrm{diag}(W_{\ddot{z}}, W_{\ddot{\theta}}, W_{\ddot{\phi}}, W_u, W_u, W_u, W_u)$$

The generalised open-loop system with scalings and weights is computed by linear operators, i.e.

$$\mathbf{G_{ol}} = \begin{bmatrix} \mathbf{W_z} \cdot \mathbf{S_z} & \mathbf{0} \\ \mathbf{0} & \mathbf{I} \end{bmatrix} \cdot \mathbf{G_{gel}} \cdot \begin{bmatrix} \mathbf{S_w} & \mathbf{0} \\ \mathbf{0} & \mathbf{I} \end{bmatrix} \tag{4}$$

B. Model Reduction of Suspension System

Observer-based modern control-design methodologies such as LQG, $\mathscr{H}_\infty$ and $\mathscr{H}_2$ are widely used in active suspension design, because they are theoretically well developed, equipped with user-friendly software, and can appropriately deal with active suspension design objectives. However, these methods typically result in controllers of an order comparable to that of the plant (possibly augmented with extra filter dynamics). Since a high-order controller is clearly impractical in most situations, e.g. to implement in economical single-chips while satisfying real-time control requirements, some approximation or model reduction techniques are essential.

Model reduction techniques attempt to approximate the dynamic model of the plant by a lower-order system easier to control. In addition, reducing the complexity of the system can offer further advantages, such as elimination of system modes irrelevant to control, simplification of the design process and the accompanying simulations, identification of crucial system characteristics, etc.

We follow the traditional model reduction approach, whereby the input-output characteristics of the plant are approximated by a lower order dynamic system, automatically resulting in lower-order controllers when modern-control methods are employed. The approximation is

TABLE II

COMPARISON OF MODEL REDUCTION APPROACHES

$norms \times 10^{-2}$		Order of reduced model					
		18	16	14	**12**	10	8
MT	$\|\|E\|\|_\infty$	15.59	15.59	17.75	52.33	82.08	85.09
	$\|\|E\|\|_H$	9.66	9.66	10.52	24.05	48.97	49.58
BT	$\|\|E\|\|_\infty$	1.35	2.09	7.19	12.22	39.50	47.83
	$\|\|E\|\|_H$	1.09	2.05	5.41	8.96	27.82	38.64
OHNR	$\|\|E\|\|_\infty$	1.09	1.05	4.56	8.17	23.26	33.01
	$\|\|E\|\|_H$	0.80	1.05	3.99	7.04	18.46	20.19

carried out sensibly so that the critical modes of the system are not highly affected. In particular, most model-reduction techniques using this approach are normally accompanied by some form of robust control-design methodology ($\mathscr{H}_\infty$ or μ) to ensure that the additional uncertainty introduced by the approximation on system has minimal effects on system stability and performance. Such a robust control method is discussed in the next section. An alternative model reduction approach is to apply approximation techniques directly to the (high-order) controller [18], but it is not considered in this work.

Three model reduction methods are utilised and compared for the reduction of the 20th order plant $\mathbf{G_{ol}}$ defined in (4), i.e. modal truncation (MT), balanced truncation (BT) [19], optimal Hankel-norm reduction (OHNR) [1].

Modal truncation is a straightforward reduction method whereby modes of the system with little influence on the dynamics of interest are removed (usually high frequency modes). The remaining poles of the MT reduced model are a subset of the original poles and thus retain their physical interpretation.

Balanced truncation first transforms the system such that the controllability P and observability Q Grammians are equal and diagonal, i.e. $P = Q = \mathrm{diag}(\sigma_1, \sigma_2, \ldots, \sigma_n)$, where σ_i are system Hankel singular values (HSVs). States corresponding to small HSVs, i.e. having less effects on the input/output characteristics of the system, can be discarded.

In the optimal Hankel norm reduction, the aim is to minimise the Hankel norm of the approximation error between the full and reduced order systems. In particular, OHNR offers better infinity norm bounds than BT. The interested reader can find more detailed discussions on the aforementioned model reduction methods in the original literature.

Table II compares the Hankel and $\mathscr{H}_\infty$ norms of the approximation errors by the different reduction methods for a number of reduced order models. MT results in the largest approximation errors, although it is easy to use (note that, due to $W_{\ddot{\phi}} = W_{\ddot{\theta}}$, the 18th and 16th order are identical for MT). OHNR gives the best results, with BT following closely in performance. Moreover, the 12th reduced order system is a good candidate for control design, as the errors increase substantially after that.

Fig. 2 shows the maximum singular value (MSV) plot of the approximation errors between the 20th full-order system and the 12th reduced-order model by the different reduction approaches. Note that the BT and OHNR produces very similar results especially within the frequency range of interest for the suspension system (1 to 10Hz).

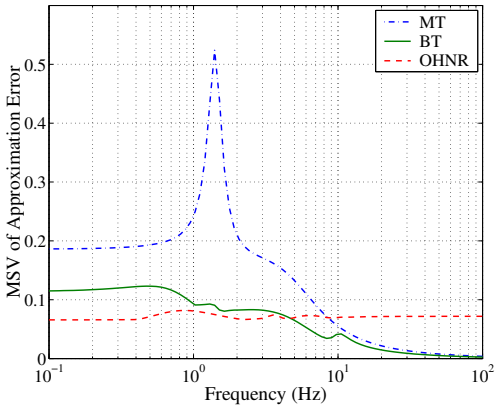

Fig. 2. Comparison of approximation errors for MT, BT and OHNR

Although the OHNR strictly gives the best 12^{th} approximation, a simple calculation of the rank indexes in (6) and (8) show that it is not suitable for applying the control method in Section III-A (i.e. no further reduction exists). However, it is possible to apply the technique in Section III-A with the BT approximate model. Thus we choose to employ the BT 12^{th}-order reduced model $\mathbf{G_{bt12}}$ for further control design. The maximum singular value between the full-order model $\mathbf{G_{ol}}$ and $\mathbf{G_{bt12}}$ can be seen in Fig. 3.

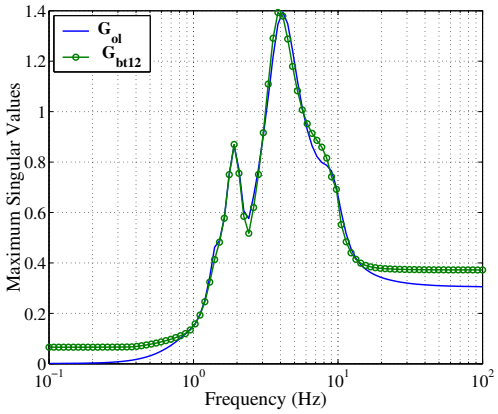

Fig. 3. System approximation

III. CONTROL DESIGN

A. Reduced $\mathscr{H}_\infty$ Control Design

Given a standard 2×2-block state-space model

$$\begin{cases} \dot{x} &= Ax + B_1 w + B_2 u \\ z &= C_1 x + D_{11} w + D_{12} u \\ y &= C_2 x + D_{21} w + D_{22} u \end{cases} \tag{5}$$

where $x \in \Re^{n_x}$, $w \in \Re^{n_w}$, $z \in \Re^{n_z}$, $u \in \Re^{n_u}$ and $y \in \Re^{n_y}$ are respectively the system state, disturbance, regulated output, control signal and measure signal vectors.

Define

$$\begin{bmatrix} M_B & N_B^T \end{bmatrix} \triangleq \begin{bmatrix} B_2 \\ D_{12} \end{bmatrix}^{\perp} \begin{bmatrix} A & \mathbf{I}_{n_x} \\ C_1 & \mathbf{0}_{n_z \times n_x} \end{bmatrix} \tag{6}$$

$$Q_B \triangleq \begin{bmatrix} B_2 \\ D_{12} \end{bmatrix}^{\perp} \begin{bmatrix} B_1 B_1^T & B_1 D_{11}^T \\ D_{11} B_1^T & D_{11} D_{11}^T - \mathbf{I}_{n_z} \end{bmatrix} \begin{bmatrix} B_2 \\ D_{12} \end{bmatrix}^{\perp T} \tag{7}$$

$$\begin{bmatrix} M_C & N_C^T \end{bmatrix} \triangleq \begin{bmatrix} C_2^T \\ D_{21}^T \end{bmatrix}^{\perp} \begin{bmatrix} A^T & \mathbf{I}_{n_x} \\ B_1^T & \mathbf{0}_{n_w \times n_x} \end{bmatrix} \tag{8}$$

$$Q_C \triangleq \begin{bmatrix} C_2^T \\ D_{21}^T \end{bmatrix}^{\perp} \begin{bmatrix} C_1^T C_1 & C_1^T D_{11} \\ D_{11}^T C_1 & D_{11}^T D_{11} - \mathbf{I}_{n_w} \end{bmatrix} \begin{bmatrix} C_2^T \\ D_{21}^T \end{bmatrix}^{\perp T} \tag{9}$$

$$\tag{10}$$

A singular value decomposition to M_B yields

$$\begin{aligned} M_B &= U_{MB} \begin{bmatrix} \Sigma_{MB} & \mathbf{0} \\ \mathbf{0} & \mathbf{0} \end{bmatrix} V_{MB}^T \\ &= \begin{bmatrix} U_{MB1} & U_{MB2} \end{bmatrix} \begin{bmatrix} \Sigma_{MB} & \mathbf{0} \\ \mathbf{0} & \mathbf{0} \end{bmatrix} \begin{bmatrix} V_{MB1}^T \\ V_{MB2}^T \end{bmatrix} \\ &= U_{MB1} \Sigma_{MB} V_{MB1}^T \end{aligned}$$

where the matrices are of compatible dimensions.

Then, we can apply a transformation to matrix $X \in \Re^{n_x \times n_x}$ as follows

$$\bar{X} = V_{MB}^T X V_{MB} \triangleq \begin{bmatrix} X_{11} & X_{12} \\ X_{21} & X_{22} \end{bmatrix}$$

Similarly, we can define the following matrices:

- For matrix N_B:

$$N_B = U_{NB} \begin{bmatrix} \Sigma_{NB} & \mathbf{0} \\ \mathbf{0} & \mathbf{0} \end{bmatrix} V_{NB}^T = U_{NB1} \Sigma_{NB} V_{NB1}^T$$

$$\bar{X} = U_{NB}^T X U_{NB} \triangleq \begin{bmatrix} X_{11} & X_{12} \\ X_{21} & X_{22} \end{bmatrix}$$

- For matrix M_C:

$$M_C = U_{MC} \begin{bmatrix} \Sigma_{MC} & \mathbf{0} \\ \mathbf{0} & \mathbf{0} \end{bmatrix} V_{MC}^T = U_{MC1} \Sigma_{MC} V_{MC1}^T$$

$$\bar{X} = V_{MC}^T X V_{MC} \triangleq \begin{bmatrix} X_{11} & X_{12} \\ X_{21} & X_{22} \end{bmatrix}$$

- For matrix N_C:

$$N_C = U_{NC} \begin{bmatrix} \Sigma_{NC} & \mathbf{0} \\ \mathbf{0} & \mathbf{0} \end{bmatrix} V_{NC}^T = U_{NC1} \Sigma_{NC} V_{NC1}^T$$

$$\bar{X} = U_{NC}^T X U_{NC} \triangleq \begin{bmatrix} X_{11} & X_{12} \\ X_{21} & X_{22} \end{bmatrix}$$

Now we are in a position to give an explicit algorithm for reduced $\mathscr{H}_\infty$ control. Interested readers can refer to [13] for the proof.

Algorithm 1: Let a system G has a minimal state-space representation given in (5). Assume that (A, B_2, C_2) is stabilisable and detectable, and $D_{22} = 0$.

1) Compute the ranks of matrices M_B, N_B, M_C and N_C. Define n_k as the minimal value of the ranks. Now, the $\mathscr{H}_\infty$ control problem is categorised into the following four cases:
   - M_B Case if $n_k = \text{rank}(M_B)$
   - N_B Case if $n_k = \text{rank}(N_B)$
   - M_C Case if $n_k = \text{rank}(M_C)$
   - N_C Case if $n_k = \text{rank}(N_C)$
2) Setup one of the following four sets of LMIs. Solve the LMIs as a feasible problem and obtain the associated matrices by using `feasp.m` in MATLAB LMI Control Toolbox.
   a) M_B Case:

$$\begin{aligned} &\mathbf{Sym}(U_{MB1} \Sigma_{MB}, X_{11}, V_{MB1}^T N_B) + \\ &\quad \mathbf{Sym}(U_{MB1} \Sigma_{MB}, X_{12}, V_{MB2}^T N_B) + Q_B < 0 \end{aligned} \tag{11}$$

$$M_C Y N_C + (M_C Y N_C)^T + Q_C < 0 \tag{12}$$

$$\begin{bmatrix} X_{11} & X_{12} & V_{MB1}^T \\ X_{12}^T & X_{22} & V_{MB2}^T \\ V_{MB1} & V_{MB2} & Y \end{bmatrix} \geq 0 \tag{13}$$

   b) N_B Case:

$$\begin{aligned} &\mathbf{Sym}(M_B U_{NB1}, X_{11}, \Sigma_{NB} V_{NB1}^T) + \\ &\quad \mathbf{Sym}(M_B U_{NB2}, X_{12}^T, \Sigma_{NB} V_{NB1}^T) + Q_B < 0 \end{aligned} \tag{14}$$

$$M_C Y N_C + (M_C Y N_C)^T + Q_C < 0 \tag{15}$$

$$\begin{bmatrix} X_{11} & X_{12} & U_{NB1}^T \\ X_{12}^T & X_{22} & U_{NB2}^T \\ U_{NB1} & U_{NB2} & Y \end{bmatrix} \geq 0 \tag{16}$$

   c) M_C Case:

$$M_B X N_B + (M_B X N_B)^T + Q_B < 0 \tag{17}$$

$$\begin{aligned} &\mathbf{Sym}(U_{MC1} \Sigma_{MC}, Y_{11}, V_{MC1}^T N_C) + \\ &\quad \mathbf{Sym}(U_{MC1} \Sigma_{MC}, Y_{12}, V_{MC2}^T N_C) + Q_C < 0 \end{aligned} \tag{18}$$

$$\begin{bmatrix} X & V_{MC1} & V_{MC2} \\ V_{MC1}^T & Y_{11} & Y_{12} \\ V_{MC2}^T & Y_{12}^T & Y_{22} \end{bmatrix} \geq 0 \tag{19}$$

   d) N_C Case:

$$M_B X N_B + (M_B X N_B)^T + Q_B < 0 \tag{20}$$

$$\begin{aligned} &\mathbf{Sym}(M_C U_{NC1}, Y_{11}, \Sigma_{NC} V_{NC1}^T) + \\ &\quad \mathbf{Sym}(M_C U_{NC2}, Y_{12}^T, \Sigma_{NC} V_{NC1}^T) + Q_C < 0 \end{aligned} \tag{21}$$

$$\begin{bmatrix} X & U_{NC1} & U_{NC2} \\ U_{NC1}^T & Y_{11} & Y_{12} \\ U_{NC2}^T & Y_{12}^T & Y_{22} \end{bmatrix} \geq 0 \tag{22}$$

   If the LMIs are not feasible, it is impossible to design an H_∞ controller for such a system.
3) Compute two full-column-rank matrices $M, N \in \Re^{n_x \times n_k}$ such that $MN^T = \mathbf{I}_{n_x} - XY$, where $\text{rank}(I - XY) = n_k \leqslant n_x$.
   a) M_B Case:
   Define

$$Z \triangleq \begin{bmatrix} X_{11} & X_{12} \\ X_{12}^T & X_{22} \end{bmatrix} - V_{MB}^T Y^{-1} V_{MB} \triangleq \begin{bmatrix} Z_{11} & Z_{12} \\ Z_{12}^T & Z_{22} \end{bmatrix}$$

Then, we have

$$X = V_{MB}\begin{bmatrix} X_{11} & X_{12} \\ X_{12}^T & X_{22} - Z_{22} + Z_{12}^T Z_{11}^+ Z_{12} \end{bmatrix} V_{MB}^T$$

b) N_B Case:

$$Z \triangleq \begin{bmatrix} X_{11} & X_{12} \\ X_{12}^T & X_{22} \end{bmatrix} - U_{NB}^T Y^{-1} U_{NB} \triangleq \begin{bmatrix} Z_{11} & Z_{12} \\ Z_{12}^T & Z_{22} \end{bmatrix}$$

$$X = U_{MB}\begin{bmatrix} X_{11} & X_{12} \\ X_{12}^T & X_{22} - Z_{22} + Z_{12}^T Z_{11}^+ Z_{12} \end{bmatrix} U_{MB}^T$$

c) M_C Case:

$$Z \triangleq \begin{bmatrix} Y_{11} & Y_{12} \\ Y_{12}^T & Y_{22} \end{bmatrix} - V_{MC}^T Y^{-1} V_{MC} \triangleq \begin{bmatrix} Z_{11} & Z_{12} \\ Z_{12}^T & Z_{22} \end{bmatrix}$$

$$Y = V_{MC}\begin{bmatrix} Y_{11} & Y_{12} \\ Y_{12}^T & Y_{22} - Z_{22} + Z_{12}^T Z_{11}^+ Z_{12} \end{bmatrix} V_{MC}^T$$

d) N_C Case:

$$Z \triangleq \begin{bmatrix} Y_{11} & Y_{12} \\ Y_{12}^T & Y_{22} \end{bmatrix} - U_{NC}^T Y^{-1} U_{NC} \triangleq \begin{bmatrix} Z_{11} & Z_{12} \\ Z_{12}^T & Z_{22} \end{bmatrix}$$

$$Y = U_{NC}\begin{bmatrix} Y_{11} & Y_{12} \\ Y_{12}^T & Y_{22} - Z_{22} + Z_{12}^T Z_{11}^+ Z_{12} \end{bmatrix} U_{NC}^T$$

4) X_{cl} is obtained as the unique solution of the linear equation $\begin{bmatrix} T & I \\ N^T & 0 \end{bmatrix} = X_{cl}\begin{bmatrix} I & S \\ 0 & M^T \end{bmatrix}$.
5) By using `basiclmi.m` in MATLAB, we can solve

$$\Psi_{X_{cl}} + \mathscr{Q}^T \Theta^T \mathscr{P}_{X_{cl}} + \mathscr{P}_{X_{cl}}^T \Theta \mathscr{Q} < 0$$

for the controller parameter $\Theta = \begin{bmatrix} A_k & B_k \\ C_k & D_k \end{bmatrix}$, where

$$\Psi_{X_{cl}} \triangleq \begin{bmatrix} A_o^T X_{cl} + X_{cl} A_o & X_{cl} B_o & C_o^T \\ B_o^T X_{cl} & -I & D_{11}^T \\ C_o & D_{11} & -I \end{bmatrix}$$
$$\mathscr{Q} \triangleq \begin{bmatrix} \mathscr{C} & \mathscr{D}_{21} & \mathbf{0}_{(n_k+n_y)\times n_z} \end{bmatrix}$$
$$\mathscr{P}_{X_{cl}} \triangleq \begin{bmatrix} \mathscr{B}^T X_{cl} & \mathbf{0}_{(n_k+n_u)\times n_w} & \mathscr{D}_{12}^T \end{bmatrix}$$

and
$A_o = \begin{bmatrix} A & \mathbf{0}_{n_x\times n_k} \\ \mathbf{0}_{n_k\times n_x} & \mathbf{0}_{n_k\times n_k} \end{bmatrix}$, $B_o = \begin{bmatrix} B_1 \\ \mathbf{0}_{n_k\times n_w} \end{bmatrix}$, $C_o = \begin{bmatrix} C_1 & \mathbf{0}_{n_z\times n_k} \end{bmatrix}$
$\mathscr{B} = \begin{bmatrix} \mathbf{0}_{n_x\times n_k} & B_2 \\ \mathbf{I}_{n_k} & \mathbf{0}_{n_k\times n_u} \end{bmatrix}$, $\mathscr{C} = \begin{bmatrix} \mathbf{0}_{n_k\times n_x} & \mathbf{I}_{nk} \\ C_2 & \mathbf{0}_{n_y\times n_k} \end{bmatrix}$
$\mathscr{D}_{12} = \begin{bmatrix} \mathbf{0}_{n_z\times n_k} & D_{12} \end{bmatrix}$, $\mathscr{D}_{21} = \begin{bmatrix} \mathbf{0}_{n_k\times n_w} \\ D_{21} \end{bmatrix}$.

6) Obtain the controller $K = D_k + C_k(sI - A_k)^{-1}B_k$ so that the closed-loop system satisfying $\|\mathscr{F}_l(G,K)\|_\infty \le 1$.

Remark 1: This algorithm is mainly based on [13], in which only the procedures for the M_B case was given. This algorithm simplifies the results in [13], and presents an explicit procedure for four cases. Hence, it is of great interest for engineering applications.

Remark 2: The LMIs given in (11) $\sim$ (22) can be obtained in a straightforward manner. For example,

$$\begin{aligned} M_B X N_B &= U_{MB1}\Sigma_{MB} V_{MB1}^T V_{MB} \bar{X} V_{MB}^T N_B \\ &= U_{MB1}\Sigma_{MB}\begin{bmatrix} \mathbf{I} & \mathbf{0} \end{bmatrix}\begin{bmatrix} X_{11} & X_{12} \\ X_{21} & X_{22} \end{bmatrix}\begin{bmatrix} V_{MB1}^T \\ V_{MB2}^T \end{bmatrix} N_B \\ &= U_{MB1}\Sigma_{MB}(X_{11}V_{MB1}^T + X_{12}V_{MB2}^T)N_B \end{aligned}$$

Hence, the standard LMI

$$M_B X N_B + (M_B X N_B)^T + Q_B < 0 \qquad (23)$$

can be transformed into (11).

B. Reduced $\mathscr{H}_\infty$ Control of Active Suspension

We now design a reduced $\mathscr{H}_\infty$ controller for the active suspension systems. The design is based on the 12th-order active suspension model, denoted by $\mathbf{G_{bt12}}$, which is designed in Section II-B by the balanced truncation method.

Since the ranks of M_B, N_B, M_C and N_C (defined in (6) and (8)) for $\mathbf{G_{bt12}}$ are $[12,\ 12,\ 12,\ 9]$, the reduced $\mathscr{H}_\infty$ control of $\mathbf{G_{bt12}}$ is treated as an "N_C Case" and a 9th-order controller $\mathbf{K_9}$ is designed for it by Algorithm 1.

For the purpose of performance comparison, the full-order controller $\mathbf{K_{20}}$ based on the model $\mathbf{G_{ol}}$ (20^{th}-order) and $\mathbf{K_{12}}$ on $\mathbf{G_{bt12}}$ are also designed. It is of interest to notice that the time for searching a feasible solution to the LMIs (denoted by t_{LMI}) and for reconstructing a controller (denoted by t_{ctr}) are quite different as shown in Table III. Note that the total time for $\mathbf{K_9}$ is only 0.541% of that for $\mathbf{K_{20}}$. It strongly demonstrates how significantly model reduction can reduce the burden of model-based controller design especially for a high-order system.

TABLE III
TIME FOR $\mathscr{H}_\infty$ CONTROLLER DESIGN IN A PENTIUM-4 COMPUTER

Controller	t_{LMI} (s)	t_{ctr} (s)	Total time (s)	Percentage
$\mathbf{K_{20}}$	5.047	81.848	86.895	100 %
$\mathbf{K_{12}}$	0.120	0.922	1.042	1.199 %
$\mathbf{K_9}$	0.090	0.380	0.470	0.541 %

Once the controller $\mathbf{K_9}$ is designed, a question is raised naturally: Can the controller be further reduced with little performance deterioration? As always, we first take an examination of the Hankel singular values of $\mathbf{K_9}$:

$$\sigma(\mathbf{K_9}) = 10^4 \cdot [5.973,\ 2.876,\ 2.331,\ 2.229,\ 2.192,\ 1.807,\ 0.069,\ 0.037,\ 0.019]$$

Based on the singular values, we can reduce the controller by order 3 as the last three singular values are much less than the rest. However, when the closed-loop system performance is considered, we decide only to reduce the controller by order 2 so that system performance is less deteriorated. Hence, the controller design process is concluded with a 7th-order controller $\mathbf{K_7}$.

IV. SIMULATION RESULTS AND ANALYSES

In this section, computer simulations are carried out to evaluate the performance of the reduced $\mathscr{H}_\infty$ controller $\mathbf{K_7}$ for the full vehicle suspension system. For a proper assessment the following five systems are compared.

- PSS: Passive suspension system $\mathbf{G_{pss}}$.
- FASS: Active suspension system with a full-order $\mathscr{H}_\infty$ controller (designed on the 20^{th} order suspension model), i.e. $\mathscr{F}_l(\mathbf{G_{gel}}, \mathbf{K_{20}})$.
- RASS-12: Active suspension system with a 12^{th} order $\mathscr{H}_\infty$ controller (designed on the 12^{th} order suspension model), i.e. $\mathscr{F}_l(\mathbf{G_{gel}}, \mathbf{K_{12}})$.

- RASS-9: Active suspension system with a 9^{th} order $\mathscr{H}_\infty$ controller (designed on the 9^{th} order suspension model in Section III-B), i.e. $\mathscr{F}_l(\mathbf{G_{gel}}, \mathbf{K_9})$.
- RASS-7: Active suspension system with a 7^{th} order $\mathscr{H}_\infty$ controller (the concluded controller in Section III-B), i.e. $\mathscr{F}_l(\mathbf{G_{gel}}, \mathbf{K_7})$.

A. Frequency Response Simulations

We first look at the frequency responses of the five suspension systems. Due to limited space, we only choose two typical frequency response plots as shown in Fig.4 and Fig.5.

Fig.4 shows the frequency response magnitude of the vehicle vertical acceleration to front-right road disturbance. It is clear that the accelerations of all the active suspension systems, compared to PSS, are considerably mitigated in the frequency range $1 \sim 10$ Hz, where people are more sensitive to vibrations. Roughly speaking, the ride performance of the active suspensions FASS, RASS-12, RASS-9, RASS-7 are very close. Note that, the frequency response magnitude of all the systems are the same around 9 Hz, i.e. the resonant frequency of the unsprung mass (wheels and tyres), because the unsprung mass is out of suspension control loop and the active suspension cannot change its inherit characteristics.

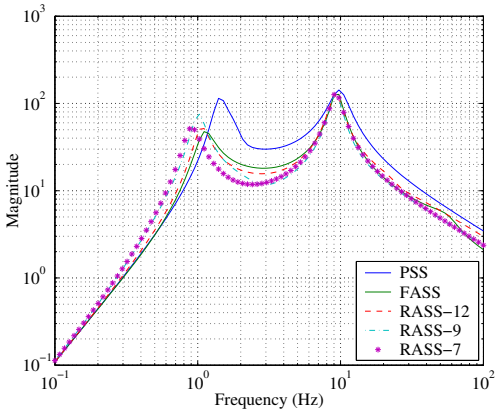

Fig. 4. Bode plot of vertical acceleration to front-left road disturbance.

Fig.5 shows the frequency response magnitude of the vehicle front-right suspension deflection to roll moment disturbance caused by driver manoeuvrers such as a sharp turn. We can observe that, at frequencies below 6 Hz, the active suspension systems have no larger suspension deflection than the passive one, and RASS-12 and RASS-9 even have less deflections in this frequency range. However, at the frequencies above 6 Hz, the active suspensions have much larger suspension deflections, especially a peak around 9 Hz. This is due to the so called "water bed" phenomenon [20]. Note that, we usually expect large suspension deflections of active systems, which is acceptable as long as suspension deflections are within a suitable bounded space. At high frequencies, the PSS, RASS-9, RASS-7 systems have similar suspension deflection responses while the FASS and RASS-12 have larger deflections. The RASS-7 system in general has the best suspension deflection response among the active suspension systems.

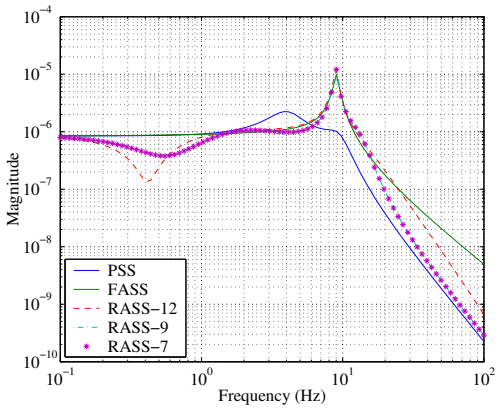

Fig. 5. Bode plot of the front-left suspension deflection to roll moment disturbance.

B. Minor-Road Test Simulations

We now assess the performance of active suspension systems under a typical road-test scenario: the vehicle is travelling on a minor road at a longitudinal speed $V_x = 20$ m/s. Since the frequency-domain comparison of the different active suspension systems have been made in Section IV-A, we put a more emphasis on the comparison between PSS and RASS-7.

Here a more precise approximation of minor road profiles is utilised:

$$S_{rd}(\Omega) = \begin{cases} C_{rd}(\Omega_{co}/\Omega_0)^{-N_1}, & \Omega \in [0, \Omega_{co}) \\ C_{rd}(\Omega/\Omega_0)^{-N_1}, & \Omega \in [\Omega_{co}, \Omega_0) \\ C_{rd}(\Omega/\Omega_0)^{-N_2}, & \Omega \in [\Omega_0, \infty) \end{cases} \quad (24)$$

where S_{rd} is the PSD function for road profiles in $\mathrm{m}^3/\mathrm{cycle}$, $C_{rd} = 5.6 \times 10^{-7}$ is road roughness coefficient, $\Omega_{co} = 0.01$ clcle/m is the cut-off wavenumber, $\Omega_0 = 0.2$ clcle/m is the wavenumber where two lines intersect, and $N_1 = 3.15$ and $N_2 = 2.42$ are the slopes for low and high wavenumbers respectively [21]. Note that $\Omega = f/V_x$, where f is the frequency in Hz. The road profiles of the front wheels are regenerated, as shown in Fig. 6, and the rear ones follow the front by a time delay $\delta = l/V_x$, where the wheelbase $l = 2.8$ m.

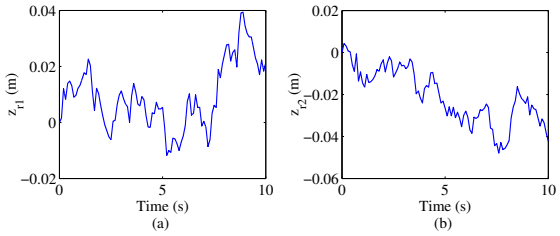

Fig. 6. Road disturbance to front wheels.

According to the ISO 2631 [16], the ride comfort level of a vehicle is quantified by the combination of the RMSs of the weighted body accelerations. In this paper, we

define the comfort index (CI) as follows:

$$\mathrm{CI} \triangleq \frac{1}{\sqrt{k_z^2 \cdot \mathrm{rms}^2(W_k \ddot{z}) + k_\theta^2 \cdot \mathrm{rms}^2(W_e \ddot{\theta}) + k_\phi^2 \cdot \mathrm{rms}^2(W_e \ddot{\phi})}}$$

where $k_z = 1$, $k_\theta = 0.4$ m/rad and $k_\phi = 0.63$ m/rad, and W_k and W_e are standard weighting functions for vertical acceleration and pitch/roll angular accelerations. Due to limited space, the expression for W_k and W_e are omitted here. Readers can refer to [16], [1] for detail.

The RMSs of the weighted vehicle body accelerations and the comfort index of all the systems are computed and listed in Table IV. It is observed from this table

TABLE IV

COMPARISON OF WEIGHTED VEHICLE ACCELERATIONS

	PSS	FASS	RASS-12	RASS-9	RASS-7
$\mathrm{rms}(W_k \ddot{z})$	0.110	0.069	0.068	0.078	0.069
$\mathrm{rms}(W_e \ddot{\theta})$	0.130	0.013	0.016	0.062	0.063
$\mathrm{rms}(W_e \ddot{\phi})$	0.167	0.030	0.068	0.114	0.114
CI	6.227	13.893	12.423	9.170	9.712

that the full active suspension system achieve the best ride comfort level while the passive one has the worst. The comfort index of RASS-7 is 30.1% less than the full active suspension system, but it is still 60.0% larger than the passive one. The RASS-7 does achieve excellent ride comfort considering that the order of the RASS-7 is reduced to nearly one third of the full order.

In summary, the 7th-order $\mathscr{H}_\infty$ controller $\mathbf{K_7}$ for the full-vehicle active suspension system achieves efficient performance although its order is reduced to approximately one third of a full controller.

V. CONCLUSIONS AND FUTURE WORKS

This paper designed a reduced $\mathscr{H}_\infty$ controller for a full-vehicle suspension system by employing the balanced truncation and direct $\mathscr{H}_\infty$ control methods throughout the whole controller design process. The reduced control, with size nearly one third of a full controller, achieved a level of performance comparable to the full one. This research demonstrates that a careful selection and integrated application of different reduction methods can achieve exceptional performance which no single method can nearly touch at its best.

This paper summarised an explicit and complete algorithm for reduced $\mathscr{H}_\infty$ control of continuous-time systems. The advantage of the algorithm is its applicability to both singular and non-singular systems. However, this algorithm cannot guarantee whether or how much the controller can be reduced.

Future work will be on a hardware-in-the-loop active suspension framework. It will be of great interest to implement the results in this framework, and undoubtedly only in a real-time application can the advantages of the reduced control design be fully explored.

VI. ACKNOWLEDGMENTS

This research was supported in part under The China-UK Science Network Scheme funded by Natural Science Foundation of China (NSFC) under Grant No. 50610105001 and Royal Society of UK (RS) under Grant No. 16852, sponsored in part by NSFC under Grant No. 60604013, and sponsored in part by Scientific Research Foundation for Returned Overseas Scholars by State Education Ministry of China.

REFERENCES

[1] J. Wang, W. Xu, and W. Chen, "Optimal Hankel-norm reduction of active suspension model," *International Journal of Vehicle Design*, vol. 40, no. 1-3, pp. 175–195, 2006.

[2] B. Lohmann, "Application of model order reduction to a hydropneumatic vehicle suspension," *IEEE Transactions on Control Systems Technology*, vol. 3, no. 1, pp. 102–109, 1995.

[3] C. Kim and P. I. Ro, "An accurate full car ride model using model reducing techniques," *Journal of Mechanical Design*, vol. 124, no. 12, pp. 697–705, 2002.

[4] Z. Liu and J. Wagner, "Nonlinear model reduction for dynamic and automotive system descriptions," *Journal of Dynamic Systems, Measurement, and Control*, vol. 24, no. 12, pp. 637–647, 2002.

[5] K. Hayakawa, K. Matsumoto, M. Yamashita, Y. Suzuki, K. Fujimori, and H. Kimura, "Robust H_∞-output feedback control of decoupled automobile active suspension systems," *IEEE Transactions on Automatic Control*, vol. 44, no. 2, pp. 392–396, 1999.

[6] J. Wang and D. A. Wilson, "Mixed $GL_2/H_2/GH_2$ control with pole placement and its application to vehicle suspension systems," *International Journal of Control*, vol. 74, no. 13, pp. 1353–1369, 2001.

[7] M. Lakehal-Ayat, S. Diop, and E. Fenaux, "An improved active suspension yaw rate control," in *Proceedings of the American Control Conference*, 2002, pp. 863–868.

[8] K. M. Grigoriadis and R. E. Skelton, "Lower-order control design for LMI problems using alternating projection methods," *Automatica*, vol. 32, no. 8, pp. 1117–1125, 1996.

[9] T. Watanabe and A. A. Stoorvogel, "Plant zero structure and further order reduction of a singular h infinity controller," *International Journal of Robust and Nonlinear Control*, vol. 12, no. 7, pp. 591–619, 2002.

[10] X. Xin, L. Guo, and C. B. Feng, "Reduced-order controllers for continuous and discrete-time singular h-infinity control problems based on lmi," *Automatica*, vol. 32, no. 11, pp. 1581–1585, 1996.

[11] T. Watanabe and A. A. Stoorvogel, "Relations between finite zero structure of the plant and the standard H_∞ controller order reduction," in *Proceedings of the IEEE Conference on Decision and Control*, 2001, pp. 1101–1106.

[12] T. Watanabe, "Lmi characterization of reduced-order h-infinity controllers via invariant zero structure," *Systems and Control Letters*, vol. 50, no. 3, pp. 165–181, 2003.

[13] J. Zeng, D. Lin, and P. Cheng, "Reduced-order controller design for the general h-infinity control problem," *International Journal of Systems Science*, vol. 37, no. 5, pp. 287–293, 2006.

[14] S. Ikenaga, F. L. Lewis, J. Campos, and L. Davis, "Active suspension control of ground vehicle based on a full-vehicle model," in *Proceedings of the American Control Conference*, 2000, pp. 4019–4024.

[15] C. O. Nwagboso, Ed., *Automotive sensory systems*, ser. Road Vehicle Automation. Chapman & Hall, 1993.

[16] ISO 2631-1, *Mechanical vibration and shock — Evaluation of human exposure to whole-body vibration — Part 1: General requirements*, 2nd ed., International Standards Organization, 1997.

[17] J. Wang, D. A. Wilson, W. Xu, and D. A. Crolla, "Integrated vehicle ride and handling control via active suspensions," *International Journal of Vehicle Design*, vol. 42, no. 3-4, pp. 306–327, 2006.

[18] K. Zhou and J. C. Doyle, *Essentials of Robust Control*. Prentice-Hall, Inc., 1998.

[19] S. Skogestad and I. Postlethwaite, *Multivariable Feedback Design: Analysis and Design*, 1st ed. John Wiley & Sons, Inc., 2000.

[20] J. C. Doyle, B. A. Francis, and A. R. Tannenbaum, *Feedback Control Theory*. New York, USA: Macmillan Publishing Company, 1992.

[21] D. A. Crolla, G. Firth, and D. Horton, "An introduction to vehicle dynamics," School of Mechanical Engineering, University of Leeds, Leeds, UK, 1992.